ORIGINAL PAGE IS
OF POOR QUALITY

N88-10832

53-20
12837
15P

ROCKET NOZZLE THERMAL SHOCK TESTS IN AN ARC HEATER FACILITY

James H. Painter and Ronald A. Williamson
McDonnell Douglas Astronautics Company

MF

BSTRACT

The McDonnell Douglas Astronautics Company (MDAC) has developed a rocket motor ozzle thermal-structural test technique that utilizes arc heated nitrogen to imulate a motor burn. The technique was used to test four heavily instrumented full-cale Star 48 rocket motor 2D carbon/carbon nozzle segments at conditions simulating ne predicted thermal-structural environment. All four nozzles survived the tests ithout catastrophic or other structural failures. The test technique demonstrated romise as a low cost, controllable alternative to a rocket motor firing. The echnique includes the unique capability of rapid termination in the event of failure nat allows post-test analysis.

NTRODUCTION

In February 1984 the McDonnell Douglas Astronautics Company (MDAC) Payload sist Module (PAM) failed to boost two communications satellites into their proper ansfer orbits. As part of the failure investigation, the MDAC Aero and Thermo-namics Laboratory was requested to develop a nozzle thermal-structural test chnique that utilized the High Impact Pressure (HIP) Arc Heater Facility.[1] After tensive development testing and environment calibrations, full scale truncated nical segments of 2D carbon/carbon nozzles were tested at conditions which mulated the thermal structural conditions which exist in an actual motor firing.

The objectives of these tests were to simulate the thermal structural envir-ment encountered by a carbon/carbon rocket motor nozzle during the first 8 s of burn d to rapidly terminate if any problems developed. The nozzle was instrumented to ovide analytical correlation, identify failure regions, mechanisms and sensitivity density variations with the carbon/carbon exit cone. The test technique utilized high power electric arc heater[2] operating on pure nitrogen at stagnation pressures om 0.9 to 1.4 MPa and stagnation temperatures from 5000 to 6700 K. The heated trogen was expanded to Mach 2 through a narrow annulus formed by a conical personic flow guide (SSFG) and a full scale truncated conical segment of the nozzle be tested. The expansion was designed to yield close simulation of the local ating rates and pressures encountered by the nozzle in an actual firing.

The test phase consisted of four carbon/carbon nozzle assemblies. The first st established the baseline thermal response characteristics using a standard zzle. The second nozzle had low density variations (DV's) identified using mputed Tompography (CT) inspection techniques. The third nozzle tested included personic flow guide modifications to more closely simulate flight conditions. The 's in the third nozzle were more severe than the second. The fourth nozzle which d passed stringent CT screening tests, was subjected to the same environment as mber three to ascertain its behavior in the same environment.

ANALYTICAL CONSIDERATIONS

The investigation had shown the most probable time of failure was 3 to 5 s after ignition. A maximum test duration of 8 s was established. The goal of these tests was to provide the heat flux and pressure required to simulate the temperature and temperature gradients which exist in the first 8 s of an actual motor firing. These conditions were established by extracting the temperature, heat flux and pressure from the detailed analytical model used for thermal structural response during a motor firing and then analytically determining what test conditions were required to provide an equivalent environment with the test hardware. The conditions used to establish the test specifications are shown in Figures 1 and 2.

In order to meet the thermal-structural environment specifications in the HIP arc heater facility with a 12 MW arc power limitation, it was necessary to confine the arc heated gas to the nozzle wall region. That confinement required a conical flow guide inside the 2D carbon/carbon nozzle, as shown in Figure 3, to reduce the gas flow requirement to the order of 0.5 kg/s. The flow guide outer contour (Figure 3) became a major design consideration since it controlled the gas expansion and thereby the local pressures and, to a large degree, the local heat transfer coefficients. An extensive boundary layer analysis resulted in four contours being tested in the course of this program. Only two of these contours were used in nozzle firings.

SUBSONIC FLOW GUIDES

Subsonic flow guides were designed to maintain subsonic flow to near node 56, provide a smooth flow transition from the exit of the arc heater to the annular throat and minimize the heating to the side walls. Figure 3 shows the geometry of the flow guides and their relative position during the calibration and nozzle tests. Flow from the arc heater is subsonic (Mach = 0.33) and remains subsonic (flow area increasing) until it approaches the throat region. Near the throat the area decreases to an equivalent throat diameter of approximately 2.5 cm and then increases allowing the flow to expand to supersonic velocity and lower local pressures. Pressure data indicated that the blunt nose shown in Figure 3 provided a smooth flow transition from the heater exit to the throat region. An earlier sharper nose choked the flow upstream of the intended throat and created significant pressure losses. The blunt nose also provided a significant reduction in heating to the front end.

SUPERSONIC FLOW GUIDE

The annular flow channel between the nozzle and the supersonic flow guide was designed to produce local pressures and surface temperatures to meet the nozzle thermal requirements. This was accomplished by contouring the conical section to a specified gap height.

The initial heat transfer calculations were made using the MINIVER code[3] and its cone flow option. These calculations used air properties and the surface emissivities were varied from zero to unity bracketing the required stagnation conditions. The supersonic flow guide was a severe heat sink in close proximity to the nozzle. Since the nozzle liner was 2D carbon/carbon and the initial flow guide was graphite there was a significant difference in temperature response for a short test. Consequently, it was necessary to use gas stagnation temperatures that were significantly higher than the rocket motor combustion products stagnation tempera-

ture (3550 K) in order to compensate for radiation from the nozzle to the flow guide. Subsequent calculations improved on the MINIVER predictions by using nitrogen gas properties, better conduction models, and closer approximations of the surface emissivities. These calculations indicated higher required stagnation temperatures.

Nominal nitrogen gas stagnation conditions were selected after completing arc heater calibrations to define the stagnation pressure, mass flow rate, current, voltage and stagnation enthalpy using an effective throat diameter of 3.18 cm. Combining these results with heating rate calculations, the following conditions were selected to meet the nozzle requirements: Stagnation pressure = 1.2 MPa, stagnation enthalpy = 7.9 MJ/kg, mass flow = 0.36 kg/s, and arc current = 1700 A.

The location of the annular throat was selected to yield the desired local pressures with the above stagnation conditions. The resultant throat was approximately 0.64 cm upstream of the carbon/carbon nozzle leading edge (Figure 3). The flow is nearly conic from this location to the exit of the skirt.

The inviscid flow area required to produce the desired pressure distribution along the nozzle was calculated for nitrogen gas expanding from the stagnation conditions described above. At this condition the ratio of specific heats for nitrogen is approximately 1.22. The inviscid flow area was calculated at approximately 1.27 cm axial intervals along the nozzle.

To prevent velocity and pressure decrement in the channel, the viscous boundary layer displacement thickness was calculated and added to the channel height. The calculations were performed by MDAC-HB using a boundary layer code that compares well with experimental data. Figure 4 presents the inviscid and viscous thicknesses along the channel. The displacement thickness (viscous value) must be multiplied by two to account for the boundary layer growth on both the guide wall and nozzle.

APPARATUS

The Star 48 nozzle thermal shock tests were conducted in the MDAC Arc Heater Facility.[1] The MDC-200 arc heater was used to heat nitrogen at pressures from 0.9 to 1.4 MPa to temperatures from 5000 to 6700 K. The heated gas was then expanded through hardware designed and fabricated specifically for this test program. The MDC-200 arc heater has been described previously[2] and no major modifications were made to it for these tests. The arc heater nozzle throat that controls the gas mass flow-pressure-enthalpy relationship was formed by the new flow guides with the equivalent diameter ranging from 2.54 to 3.18 cm.

ARC HEATER

The nitrogen stagnation temperature and pressure available for these thermal shock tests was determined through two series of arc heater calibrations. The first series used four power units in a series parallel arrangement. The upper arc current limit was approximately 1800 A. The second series of tests used three parallel power units in series with two parallel higher current units yielding an upper arc current limit of approximately 3000 A for periods of less than 10 s. The nozzle throat diameters for these calibrations were 2.54 and 3.18 cm.

Figure 5 shows the performance of the MDC-200 arc heater operating on nitrogen over the complete range of calibration. Data are included for two forward electrode lengths (68 and 91 cm). In general, a higher gas temperature can be achieved with the

shorter electrode and the smaller nozzle throat. Higher enthalpies can be achieved at higher arc current. As dissociation of the nitrogen begins, the gas temperature increase does not follow the rate of enthalpy increase (lower gas specific heat).

One critical test requirement was rapid stabilization. Simulation of a rocket motor firing required full flow conditions within 0.5 s of start-up. The gas flow control system and the arc current controllers in the HIP facility were modified to attempt to meet this requirement. Rapid action regulators were installed in the main gas flow lines to the arc heater and their opening rates were adjusted to achieve minimum start time without arc extinction (blow-out). Meter relays were used to sense arc current and trigger the regulator loading via solenoid valves. The arc current controllers were set to yield maximum demand on start-up and then switched to a pre-set level shortly thereafter. In later tests, a third controller was used to yield current reductions during a test. The arc heater starting characteristics shown in Figure 6 are typical of the rapid response achieved in the actual nozzle tests. The 10 to 90% rise time to full heating for the Phase I tests was 0.5 s. It was slightly longer for the Phase II tests (0.8 s) due to the higher arc current requirement.

SUPERSONIC FLOW GUIDE

Eight supersonic flow guides were fabricated with four different external contours for these tests. The first SSFG assembly was used for only one calibration test and then discarded when a crack developed in the vertical forward face of the ATJ graphite. The second configuration determined that the local pressures and heating rates were too low requiring modifications to the subsonic nose region. In the third configuration, the ATJ-S nose and centering plug were combined into a single piece and the contour was blunted significantly to avoid pressure degradations from premature accelerations. This SSFG was used to test the first nozzle. During that test, thermal stress cracks were encountered in the sonic region of the ATJ cone. The sonic region was strengthened in the fourth and fifth configurations by using ATJ-S graphite. The ATJ-S sonic region was bonded to the ATJ cone using graphite cement. This configuration was used to test the second nozzle. Again thermal stress cracks developed in the sonic region but this time there was no significant separation of the pieces. A sixth SSFG was identical to the fourth for over-test calibrations.

Subsequent thermal analysis indicated the nozzle heat flux distribution needed improvement. A new contour was specified that was aimed at reducing the heat flux in the near sonic region, holding the same flux in the mid-region and increasing the flux at the exit. This was accomplished primarily by moving the sonic point upstream 1.27 cm and decreasing the gap width over the entire flowfield. In addition to the contour change, the material of the sonic region was changed from ATJ-S to 3D carbon/carbon. Figure 7 shows the design selected to improve the thermal strength.

The seventh SSFG shown in Figure 7 was used to test the third nozzle. After 4.5 s at the higher current condition, the ATJ aft skirt failed through the three pressure ports where stainless steel fittings were used. The 3D carbon/carbon was undamaged.

The eighth and final SSFG was identical to the previous design except that graphanol pressure fittings were used and an accelerometer was added. The accelerometer was protected by RTV insulation as shown in Figure 7. This configuration was used to test the fourth nozzle for 8 s. The SSFG was in excellent condition post-test.

CALIBRATION MODULE

Calibration modules (Figure 8) were used to define the thermal environment of the nozzle. Water-cooled calorimeters and pressure taps were used in conjunction with the SSFG instrumentation to document the cold wall heating rates, local pressures and thus local heat transfer coefficients from the sonic point to the nozzle exit. The instruments were located at stations defined by thermal model nodes as numbered by the original nozzle analysis. Node 56 was the entrance to the nozzle segment, node 121 was located 6.35 cm downstream, node 151 was 10.92 cm downstream and node 186 was 16.51 cm downstream. Node 186 was essentially the end of the SSFG and node 56 was very near the sonic point in the initial tests. Node 121 was used in the early design work as the nominal target point and node 151 was a convenient distribution point between node 121 and the exit.

The first calibration module was used in nine tests to define the flowfield for Phase I nozzle tests (Figure 9). This module failed in Test 1811 after 6.4 s at the intersection of the cylindrical body and the conical skirt just downstream of the flange. The entire cone separated banging against the SSFG causing a trapazoidal segment to break loose from the main body.

The second calibration module differed from the first in two ways. First, the failure region was beefed-up by machining a large radius at the conical blend (Figure 8) and second the calorimeters were relocated to nine locations. Three calorimeters were located at node 56, three at node 121 and three at node 186. The four pressure taps were also located at nodes 56, 121 (two). and 186. This module was used to calibrate the flowfield using two different supersonic flow guides in 16 tests and remains operational.

CALIBRATION TESTS

A total of 32 calibration tests were made to define the flowfield adjacent to the nozzle segment and improve the simulation of flight conditions. The first calibration series (Tests 1802-1811) optimized the heating rates at arc currents less than 1800 A and reduced mechanical deflections of the supersonic flow guide and arc heater. The second calibration series (Tests 1824-1830) established the heating rates at arc currents to 2900 A and reduced the thermal distortion from sting heating. The third calibration series (Tests 1831-1839) documented the high current heating rates using a modified contour on the supersonic flow guide and provided data on the effects of arc current variations during a test.

CALIBRATION DATA - SERIES I

The calibration data acquired in Series I, tests 1809 to 1811, were measured with the supersonic flow guide positioned to yield an annular throat area of 6.45 cm^2. The nitrogen flow rate was 0.36 kg/s. The measured pressures agreed favorably with the predicted values and thus the nozzle design values. Figure 9 compares the local static pressures at four locations to the nozzle design pressures. These data indicate less boundary layer growth than predicted and hence slightly lower static pressures at nodes 151 and 186 than predicted. The measured cold wall heating rates were higher than desired at node 91, very close to design values at node 121 and lower than desired at nodes 151 and 186 as shown in Figure 9.

Heat transfer coefficients were derived from the cold wall heating rates, local pressures and local enthalpies. The local enthalpies were estimated from measured stagnation enthalpies and estimated wall losses upstream of the point in question. The calculated heat transfer coefficients for tests 1806 through 1811 could be correlated as proportional to the local pressure to the 0.8 power from 65 to 350 kPa.

The local heat transfer coefficients were then used to estimate the hot wall heat flux as a function of time at nodes 56 and 121. The predicted hot wall heating rates are shown in Figures 10 and 11 where they are compared to the original predictions for the nozzle to be tested. The calibration data indicates an over-test at node 56 and a good match at node 121.

CALIBRATION DATA - SERIES II

The second series of calibration tests was conducted to determine the facility over-test capability (higher heating rate). The power supplies were reconfigured to allow arc currents to 3400 A. The calorimeters were relocated in the new module to yield better axial and circumferential distributions and two more calorimeters were added. This yielded three calorimeters at node 56, three at node 121, and three at node 186. They were aligned along three rays 120° apart with rows at 22°, 142° and 262° from top center. The pressure taps were located at nodes 56, 121, 151 and 186.

Tests 1825 through 1828 were conducted at constant nitrogen flow rates and constant effective throat area while the arc current was increased from 1480 to 2750 A. The averaged local heating rates increased 33% at node 56, 43% at node 121 and 30% at node 186 as a result of the 86% increase in arc current. The nitrogen stagnation enthalpy increased 46% but due to dissociation the temperature increased only 20%. The stagnation pressure increased 15% due to the hotter gas and constant mass flow rate. The expected heat flux improvement based on the increased heat transfer coefficient the increased gas temperature and the assumption that no recombination occurs in the boundary layer would be a 31% increase. Thus increased arc current does yield predictably higher heating rates but dissociation limits the increase.

CALIBRATION DATA - SERIES III

The third calibration series provided flowfield definition for the final two nozzles tested and perfected the technique of arc current variation during a test. The supersonic flow guide contour was modified to move the sonic point 1.27 cm upstream and thus decrease the heat flux at node 56, hold the same level at node 121 and increase the flux at node 186.

The new SSFG contour improved the heat flux distribution. A comparison of the data from Series II and III shows a 10% reduction in heat flux at node 56, no change at node 121 and a 68% increase at node 186. The reduction at node 56 was not as desired but the contour was judged to be acceptable for nozzle testing.

ROCKET MOTOR NOZZLE THERMAL SHOCK TESTS

Four full-scale nozzles were subjected to the environments summarized in Table 1, simulating a rocket motor firing. These nozzles were truncated conical segments of Star 48 rocket motors fabricated using production materials processes and tooling. The objectives of these tests were to validate thermal/structural response predictions, to determine the sensitivity of these nozzles to low density regions in the 2D carbon/carbon exit cone, and to identify any failure regions and/or mechanisms.

The four nozzles tested were delivered by Morton-Thiokol with thermocouples, strain gauges and pressure transducers installed. The exit cones used in the first and fourth nozzles passed the CT screening criteria, the second and third nozzles contained exit cones which had low density regions (DV's) identified by Computed Tomography (CT) inspection techniques.

Figure 12 illustrates a typical nozzle segment. It consists of a 2D carbon/carbon truncated conical liner, a two-piece carbon/phenolic insulator, a titanium closure and a titanium adaptor ring. Two layers of carbon felt were wrapped around the outside of the downstream end. The minimum inside diameter of the 2D carbon/carbon liner was 12.2 cm and the exit inside diameter was 30.5 cm. The cone half-angle was 24°. Thermocouples, strain gauges, pressure taps and accelerometers instrumented the nozzle tests. The instrumentation was completely outboard of the 2D carbon/carbon liner. The strain gauges were outboard of the carbon phenolic insulator and the accelerometers were outboard of the titanium closure. Two pyrometers were focused on the nozzle near the SSFG exit during all four tests.

In addition to the nozzle instrumentation, each test included standard arc heater facility instruments, the SSFG instruments and displacement or deflection instruments. The standard arc heater over-pressure interlock was the primary test terminator in the event of a catastrophic nozzle failure. Three motion picture cameras were also used to record each test. The top and side cameras normally used color film. The bottom camera normally used black and white film for fast developing. The frame rates varied from 400 to 800 fps.

PHASE I - THERMAL SHOCK TESTS

The first nozzle was tested at a nitrogen stagnation temperature of 5670 K. The stagnation pressure and enthalpy are shown in Table 1. Ten thermocouples were in contact with the 2D carbon/carbon liner along two rows 180° apart. Nine thermocouples were located in the carbon phenolic insulator along two rows 180° apart and 2.5 cm circumferentially away from the liner rows. One thermocouple was located in the bottom of the locking pin hole and one near a strain gauge. Six strain gauges were bonded to the carbon phenolic insulator.

Figure 12 shows the nozzle in place prior to Test 1812. The supersonic flow guide is retracted showing its surface as well as the inside nozzle surface. The SSFG mounting sting had not yet been covered with the cylindrical heat shield in order to illustrate the mounting and alignment apparatus. The alignment of the SSFG with the nozzle was critical and great care was taken to precisely align the two cones.

In the first nozzle test the steady-state conditions were reached in 0.75 s and 90% of the full pressure in 0.50 s. The stagnation pressure increased at about 100 kPa/s during the test as the energy losses to the flow guides decreased. At 6 s into the test, there was an abrupt pressure increase. At 6.34 s, a SSFG thermocouple rapidly increased in output indicating internal gas flow. At 7.09 s the over-pressure interlock terminated the test. The pre-set test time was 8 s.

Post-test inspection revealed the ATJ graphite SSFG had failed circumferentially in the near sonic region (maximum heat flux) and a section of the guide had partially blocked the flow creating the over-pressure termination at 7.09 s. The interior of the nozzle was coated with a white deposit of zinc chromate from the nozzle region between the 2D carbon/carbon liner and the carbon phenolic "dixie cup" insulator. The asymmetric pattern was caused by a combination of SSFG deflection and

fracture. Two sections from the sonic region separated from the SSFG and wedged against the 2D carbon/carbon liner.

The test data was reviewed and an excellent temperature correlation was found for selected points. There were several obviously bad contact thermocouples. The optical pyrometer data correlated well with the analysis. Carbon phenolic temperatures reached as high as 1000 K during post-test soak.

Figure 13 compares the predicted flight surface temperatures to those derived from an analysis that included actual calibration data for and stagnation gas properties from the first nozzle test. The comparison in Figure 13 shows higher than desired temperatures at node 56, a reasonable simulation at node 121 and lower than desired temperatures at node 186.

The sonic region material of the SSFG was changed to ATJ-S graphite in an attempt to strengthen the assembly and test the full 8 s on the second nozzle. A copper spray ring was attached to the titanium closure to bathe the carbon felt in cool gaseous nitrogen and prevent post-test combustion.

The stagnation pressure was essentially constant at 1.1 MPa throughout Test 1813. The stagnation enthalpy was 7.7 MJ/kg. The slightly lower pressure resulted in slightly lower heating rates on the second nozzle than on the first. Following the test, the carbon felt was removed immediately and the SSFG was retracted much faster than the first test. As a result, the peak temperatures post-test were lower in the carbon phenolic. A low nitrogen flow rate purged the flow field post-test which also helped to reduce post-test heat soak and preserved the model for examination.

In general, the interface temperature data correlated reasonably well with the analysis (Figure 14). It was apparent that the second nozzle test ended with an asymmetric flowfield. The oxide patterns on the nozzle and the SSFG surfaces were the first indication of asymmetry and the temperaure measurements confirmed it. Additional thermal protection was incorporated on the sting and sting holder for Phase II to reduce the SSFG deflections that cause asymmetric flow.

Conclusions drawn from the Phase I tests were: (1) the test facility was capable of providing a good simulation of node 121 temperatures and pressures, (2) SSFG and/or nozzle deflections resulted in asymmetric heating, (3) temperature data indicated the desired temperature gradient was achieved in the critical area, and (4) there was no catastrophic failure of either nozzle.

PHASE II - THERMAL SHOCK TESTS

The contour of the SSFG was changed to reduce the heating rate at node 56 relative to node 121 and the stagnation temperature and pressure were increased to raise the heating rates at node 186. The increased gas temperature was achieved through significantly increased arc current and a shorter arc heater cathode. Nitrogen dissociation limited the temperature rise. An arc current of 3000 A was required to achieve a 6670 K stagnation temperature.

Twenty-two thermocouples were located along six conical rays. Four of the rows each contained four thermocouples at the carbon/carbon outside surface to yield a direct symmetry check. Five thermocouples measured carbon phenolic temperatures and one was located at the bottom of the locking pin hole. Two transducers were added to sense the venting pressure between the liner and insulator 5 cm upstream of the insulator exit and 180° apart.

The Phase II SSFG was designed to incorporate a 3D carbon/carbon sonic region. This significantly enhanced the high temperature strength of the flow guide in the high heat flux region. The contour of the SSFG was modified to move the sonic point forward of the previous location and to reduce the gaps on the entire flowfield.

In the test of the third nozzle, a stagnation pressure of 1.3 MPa was achieved in 1 s and the pressure then rose linearly to 1.4 MPa at 3.25 s followed by a decrease to 1.3 MPa at 4 s. The gas enthalpy reached 10.9 MJ/kg in 3.25 s and then was decreased to 8.1 MJ/kg for the remainder of the test. At 4.5 s into the test, the SSFG graphite aft skirt fractured and the test was manually terminated at 5.1 s.

Post-test inspection of the 2D carbon/carbon nozzle liner revealed ten delaminations on the inside surface in the high heat flux region. Two additional delaminations were just starting. The worst delamination was 5 mm deep. The effluent appeared quite symmetrical and this was verified by both temperature and pressure data. The ATJ graphite aft skirt of the SSFG fractured into several pieces. The 3D carbon/carbon sonic region held up well with only a few fibers missing from the surface. The fractures of the SSFG aft skirt were attributed to differential thermal expansion between the node 121 pressure tap fittings, which were stainless steel, and the graphite. The stainless steel fittings thermally expanded inside what was already a stress concentration at four times the graphite expansion rate causing fracture initiation. Subsequent tests used graphite fittings with aluminum oxide interior sleeves to reduce leakage.

Even though the stagnation conditions were higher than planned, the larger flowfield gap apparently resulted in lower temperatures than predicted. Figure 15 compares the predicted flight surface temperatures of the 2D carbon/carbon nozzle to those derived from an analysis that included actual calibration data for and gas state properties from the third nozzle test. The comparison in Figure 15 shows a distinct improvement in simulation over the first two nozzle tests. The temperatures are lower than desired at 5 s but higher than flight at 3 s.

Three general conclusions were reached regarding the third nozzle test: (1) the flow was symmetrical, (2) a good simulation of the surface temperature profile was produced, and (3) the temperature gradient through the carbon/carbon was in good agreement with flight predictions.

Several improvements were made in the instrumentation for the final nozzle test. Another 14-channel tape recorder was added to yield higher frequency data. Six strain gauges, three SSFG pressures, two displacement measurements, one vent pressure, one microphone and a time code were recorded on the new unit. An accelerometer was mounted inside the SSFG with elaborate heat shielding (see Figure 7). Linear potentiometer displacement transducers were attached to the nozzle to measure vertical and lateral movement.

The test plan was to achieve a stagnation pressure of 1.4 MPa and a stagnation enthalpy of 10.5 MJ/kg at 3.25 s then decrease the pressure to 1.2 MPa and enthalpy to 7.8 MJ/kg. The desired test time was 8 s. The objective was to provide a test environment as close to flight (and the third nozzle test) as possible for a nozzle that passed all acceptance criteria. The actual test conditions came very close to the planned conditions. The total test time was 8.03 s. The test conditions were virtually identical to those for the third nozzle.

There were five nozzle surface delaminations plus one just starting in the high heat flux region. They were shallow and visible only with a high intensity light. All delaminations appeared to be at the feathered end of the 2D carbon/carbon layers.

There was a significant improvement in the quality of the thermocouple data primarily due to the improved installation technique. The temperatures measured at the insulator-liner interface near the knuckle region were in reasonable agreement with the predictions. The external temperature aft of the closure was also in reasonable agreement with predictions. Temperatures measured at the downstream interface were higher than predicted but the optical pyrometer data obtained on the inner surface near that location were in good agreement with predictions.

Figure 16 compares the predicted flight surface temperatures of the 2D carbon/carbon nozzle to those derived from an analysis that included actual calibration data for and gas state properties from the fourth nozzle test. This comparison shows the best flight simulation achieved to date.

SUMMARY

The MDAC-STL Aero and Thermodynamics Laboratory developed a Rocket Motor Nozzle Thermal-Structural Test Technique utilzing the High Impact Pressure (HIP) Arc Heater Facility. The technique was then used to test four Star 48 rocket motor truncated conical nozzle segments at conditions simulating the predicted nozzle environment. Two of the nozzles had passed the new CT screening criteria and two had not. A very good simulation of the predicted thermal pulse at the forward end of the motor exit cone through 8 s of motor burn was achieved.

Significant problems with this test technique included high thermal stress on the supersonic flow guide (SSFG), deflection and thermal distortion of the SSFG sting assembly, and post-test nozzle thermal soak caused by the presence of the hot SSFG. SSFG thermocouple and pressure fitting problems also plagued the tests.

The technique developed and used in these tests has demonstrated considerable promise as a low cost alternative to a rocket motor firing for investigation of failures, screening of materials, development of new designs and batch qualification of production hardware. Further development of the technique should include advanced materials for the SSFG aft section, an improved pedestal for the SSFG to further avoid deflections, improved instrumentation inside the SSFG, and additional terminators in the event of failures.

REFERENCES

1. Rinehart, W. A., Painter, J. H., Williamson, R. A., et al, High Impact Pressure (HIP) Arc Heater Facility, 17th Anual Technical Meeting of the Institute of Environmental Sciences, Los Angles, CA 1971.

2. Painter, J. H. and Ehmsen, R. J., A 12 MW, 200 atm Arc Heater for Reentry Testing, AIAA J. 9, 2307 (1971).

3. Hender, D. A., A Miniature Version of the JA70 Aerodynamic Heating Computer Program, H800 (MINIVER), McDonnell Douglas Report MDC G0462, June 1970 (revised January 1972).

Table 1
Star 48 rocket motor nozzle segment tests

11–6269

TEST NO.	DATE	NOZZLE NO.	STAGNATION PRESSURE (MPa)	STAGNATION ENTHALPY (MJ/kg)	TEST TIME (s)	RESULTS	THERMAL STRUCTURE SIMULATION
1812	10 MAY 84	1	1.2 – 1.3	8.1	7.09	NO EXIT CONE DAMAGE.	UNDER FLIGHT PREDICTIONS.
1813	15 MAY 84	2	1.0 – 1.1	7.7	8.03	ONE SLIGHT DELAMINATION	UNDER FLIGHT PREDICTIONS.
1840	19 JUNE 84	3	1.3 – 1.4	8.1 – 10.9	5.09	TWELVE DELAMINATIONS	FLIGHT PREDICTIONS.
1841	09 JULY 84	4	1.3 – 1.4	7.7 – 10.9	8.00	SIX DELAMINATIONS	FLIGHT PREDICTIONS.

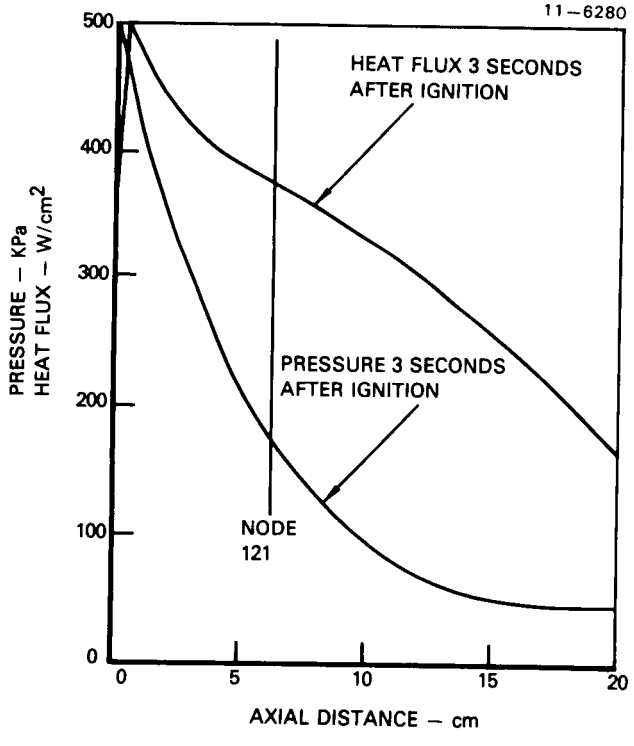

Figure 1. Nozzle surface heat flux specifications

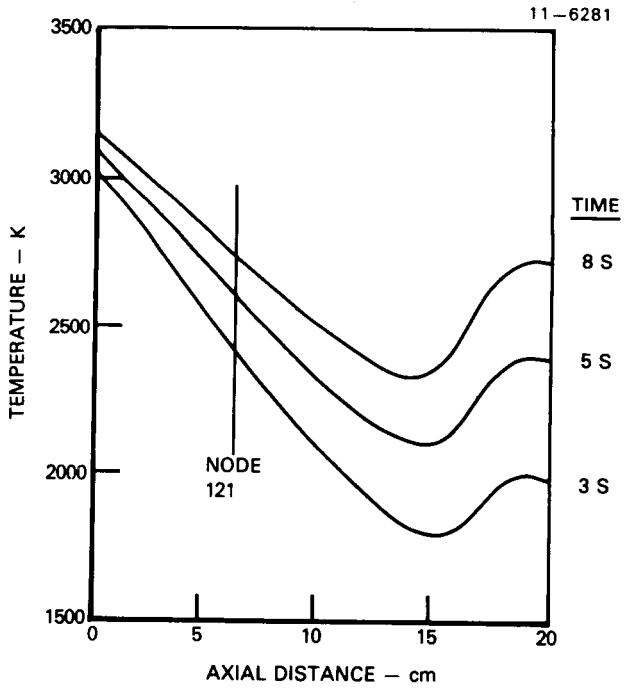

Figure 2. Nozzle surface temperature specifications

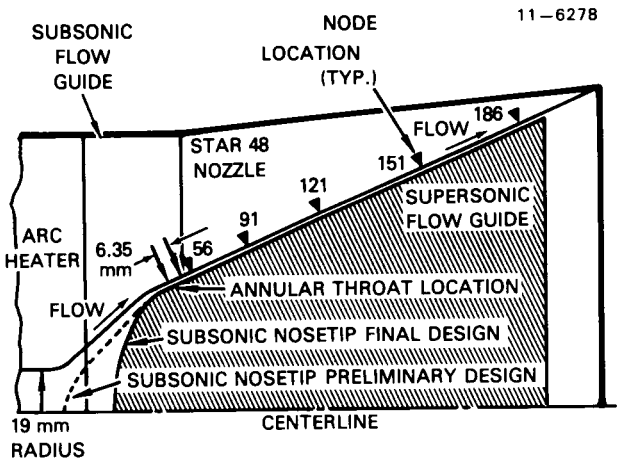

Figure 3. Schematic diagram of rocket nozzle test technique

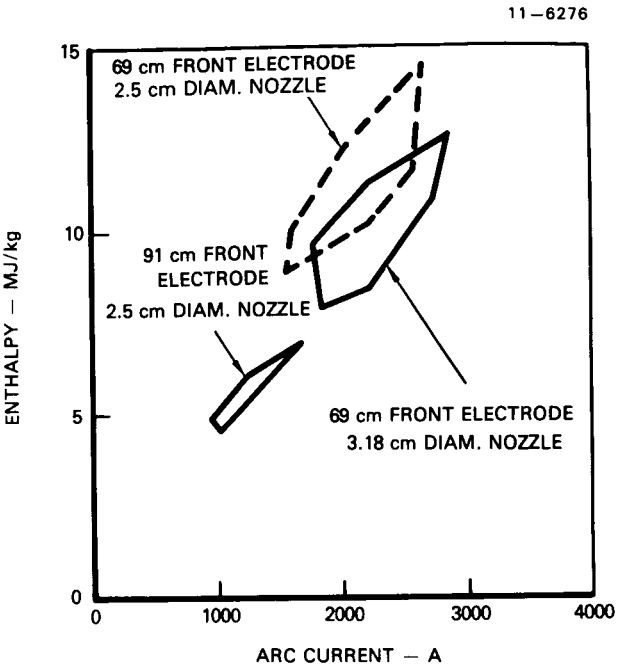

Figure 5. Arc heater calibrated enthalpy range for nozzle tests

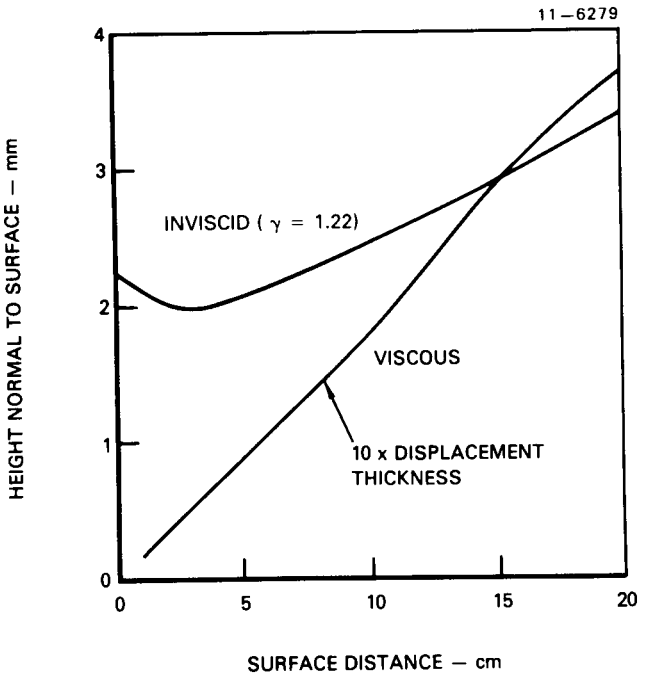

Figure 4. Flow channel height derivation

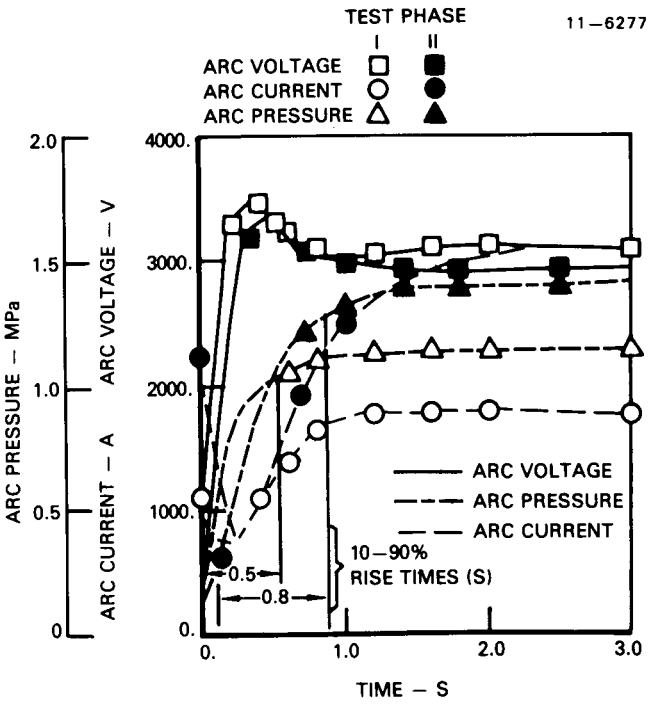

Figure 6. Arc heater start characteristics

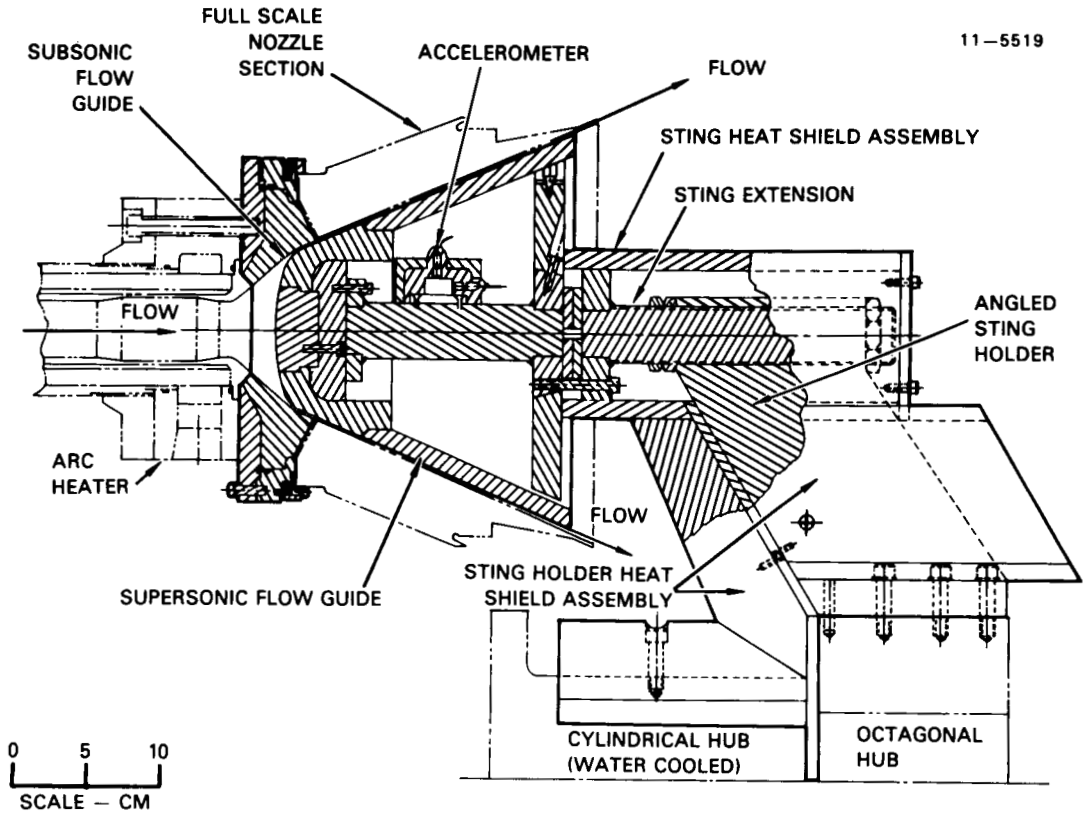

Figure 7. Flow guide assembly for phase II nozzle tests

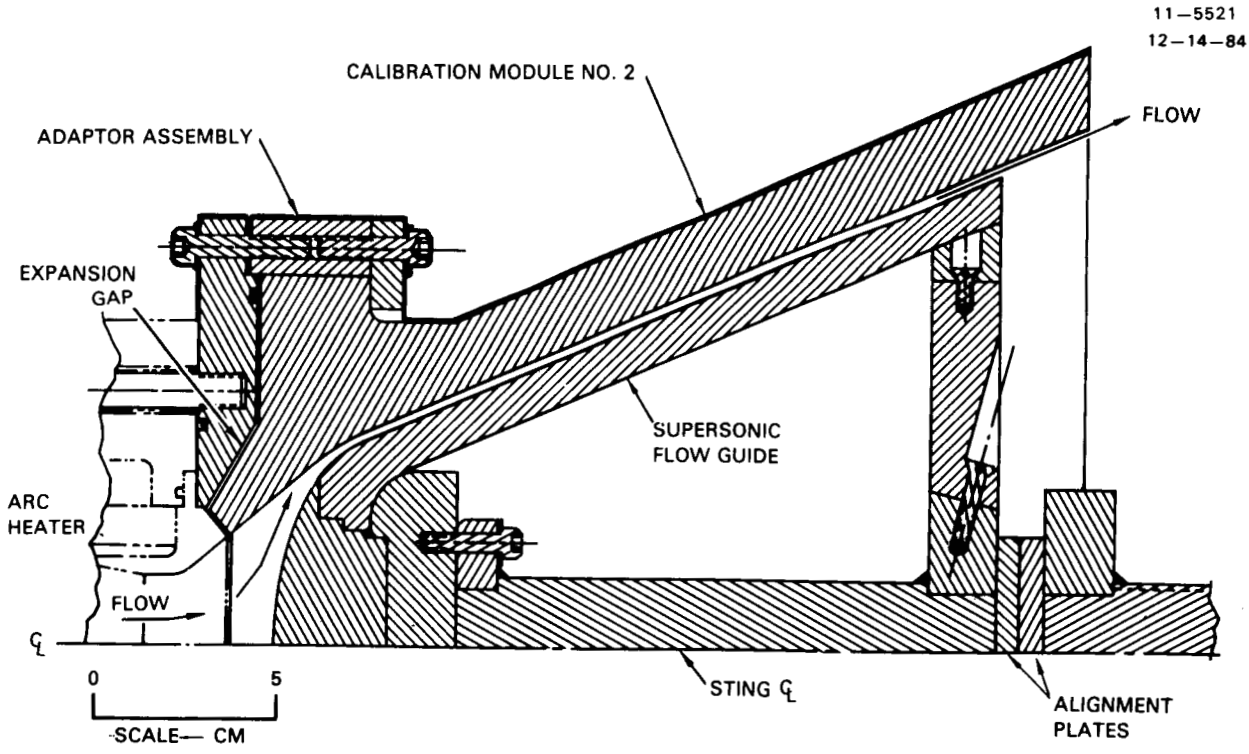

Figure 8. Nozzle environment calibration module

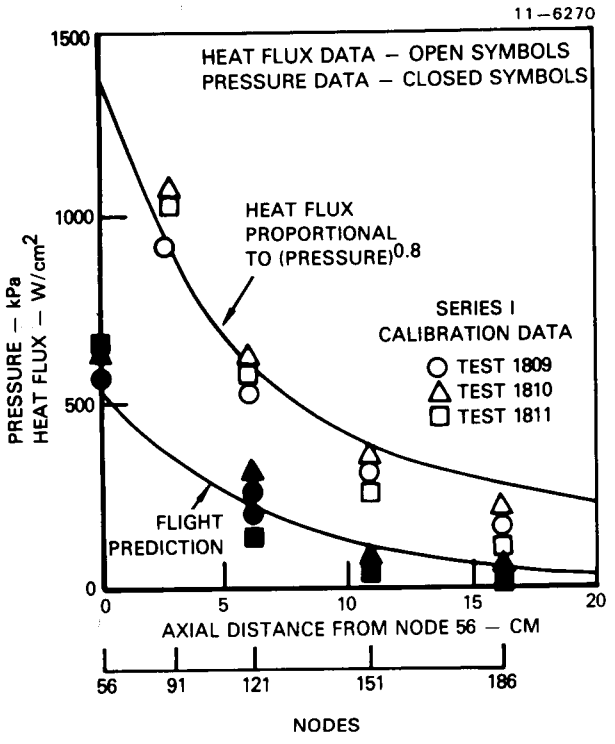

Figure 9. Heat flux profiles from calibration series I

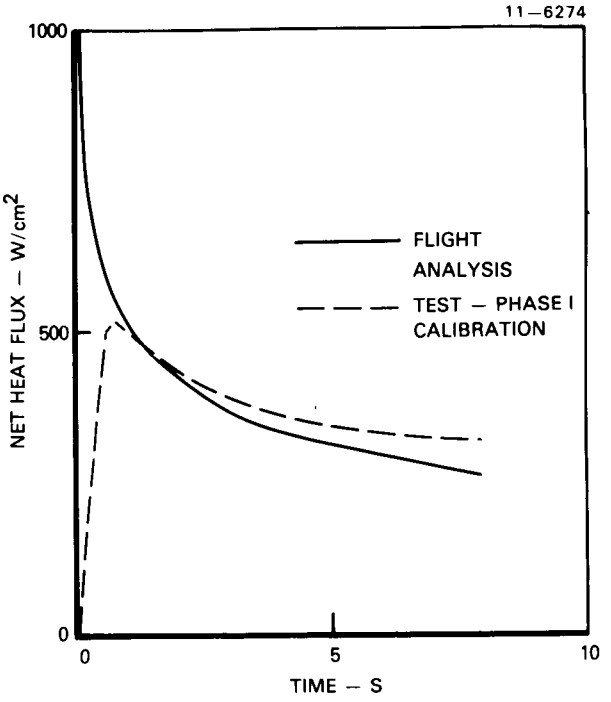

Figure 11. Comparison of flight and test heat flux predictions at node 121

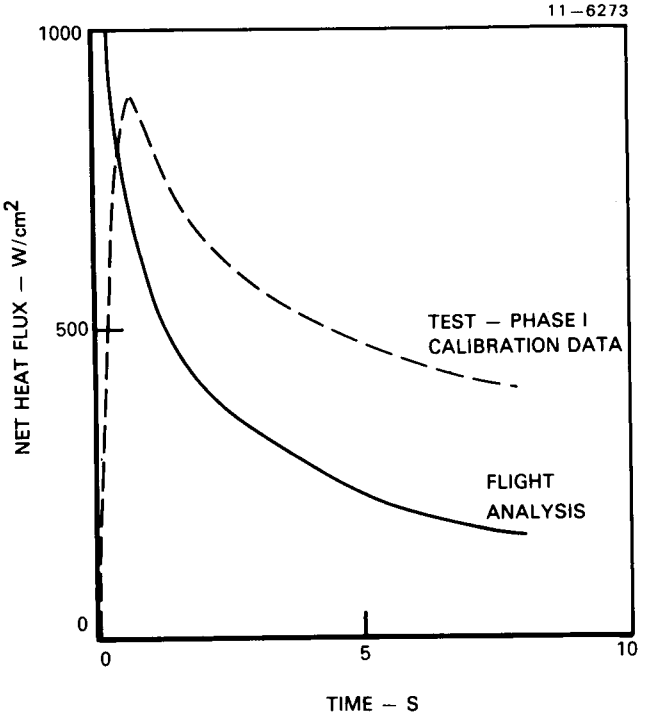

Figure 10. Comparison of flight and test heat flux at node 56

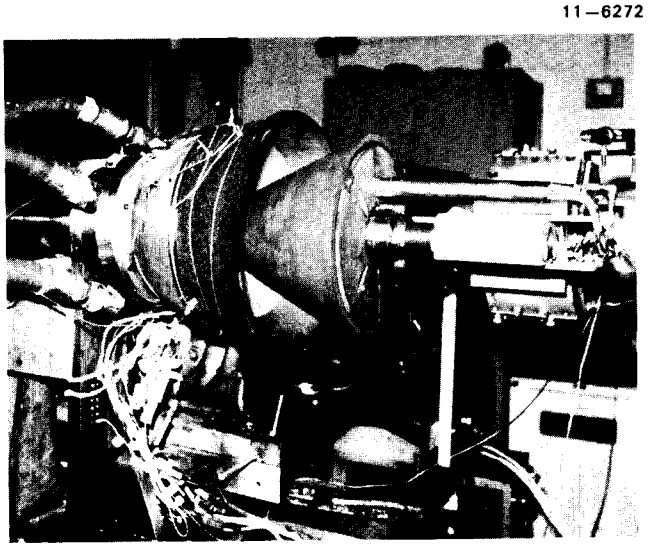

Figure 12. Nozzle test assembly

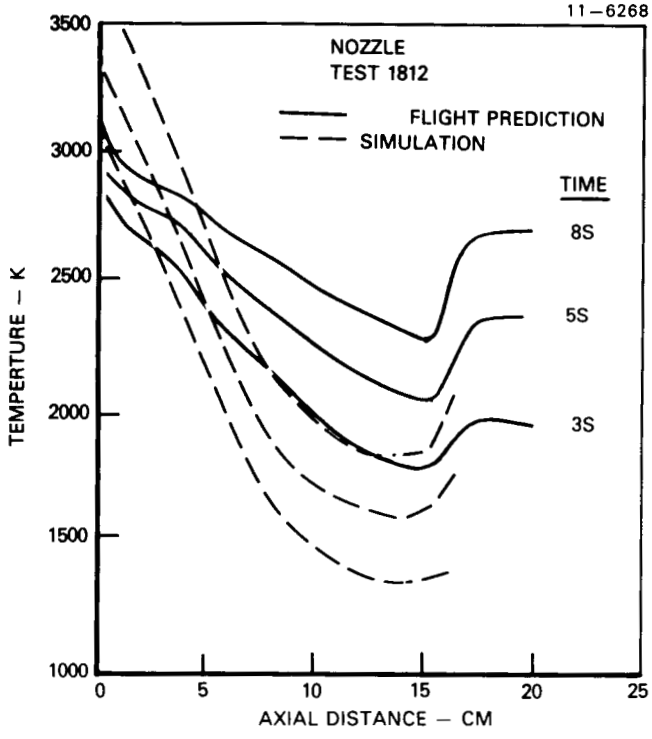

Figure 13. Comparison of nozzle surface flight temperature predictions to test 1812 simulation

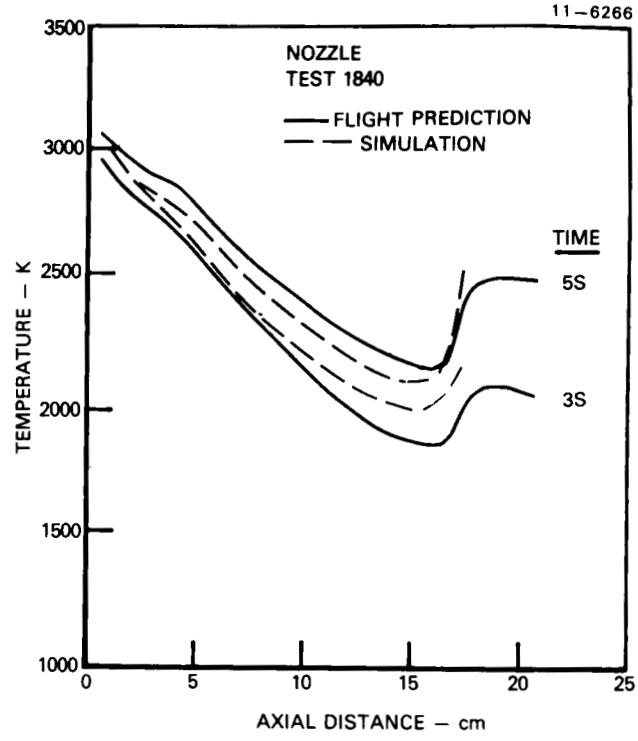

Figure 15. Comparison of nozzle surface flight temperature predictions to test 1840 simulation

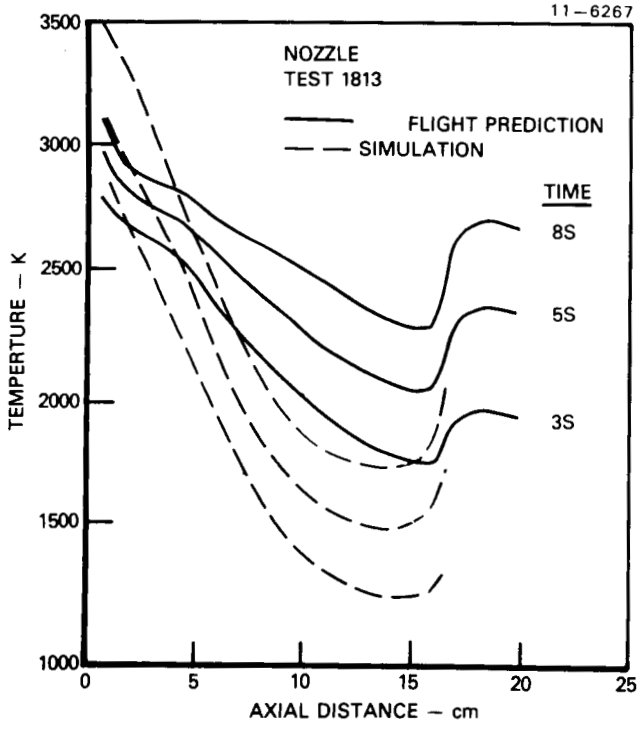

Figure 14. Comparison of nozzle surface flight temperature predictions to test 1813 simulation

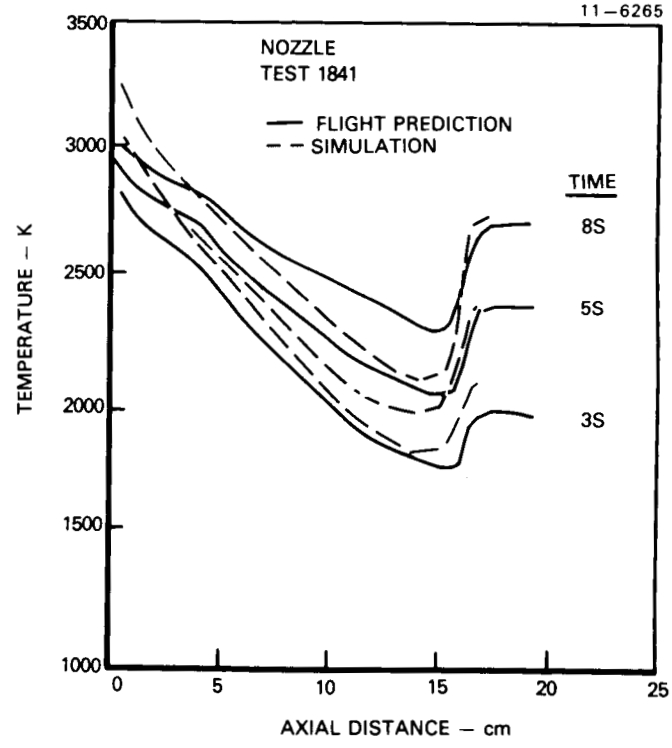

Figure 16. Comparison of nozzle surface flight temperature predictions to test 1841 simulation